

## Hot Paper

## An In Crystallo Reaction with an Engineered Cytochrome P450 Peroxygenase\*\*

Joel H. Z. Lee,<sup>[a]</sup> John B. Bruning,<sup>[b]</sup> and Stephen G. Bell<sup>\*,[a]</sup>

The cytochrome P450 monooxygenases (CYPs) are a class of heme-thiolate enzymes that insert oxygen into unactivated C–H bonds. These enzymes can be converted into peroxxygenases via protein engineering, which enables their activity to occur using hydrogen peroxide (H<sub>2</sub>O<sub>2</sub>) without the requirement for additional nicotinamide co-factors or partner proteins. Here, we demonstrate that soaking crystals of an engineered P450 peroxxygenase with H<sub>2</sub>O<sub>2</sub> enables the enzymatic reaction to occur within the crystal. Crystals of the designed P450 peroxxygenase, the T252E mutant of CYP199A4, in complex with 4-methoxybenzoic acid were soaked with different concentrations of H<sub>2</sub>O<sub>2</sub> for varying times to initiate the in crystallo O-

demethylation reaction. Crystal structures of T252E-CYP199A4 showed a distinct loss of electron density that was consistent with the O-demethylated metabolite, 4-hydroxybenzoic acid. A new X-ray crystal structure of this enzyme with the 4-hydroxybenzoic acid product was obtained to enable comparison alongside the existing substrate-bound structure. The visualisation of enzymatic catalysis in action is challenging in structural biology and the ability to initiate the reactions of P450 enzymes, in crystallo by simply soaking crystals with H<sub>2</sub>O<sub>2</sub> will enable new structural biology methods and techniques to be applied to study their mechanism of action.

## Introduction

Cytochrome P450 enzymes (P450s) are heme-thiolate monooxygenases that catalyse the selective insertion of one atom of dioxygen (O<sub>2</sub>) into C–H bonds. This enables them to catalyse a wide variety of complex transformations including epoxidation, heteroatom oxidation, desaturation, dealkylations, and C–C bond cleavage and formation.<sup>[1]</sup> The sequence identity between P450s from different families and species can vary widely as can their substrate range but their overall structures are broadly conserved. Their spectroscopic properties are similar due to the heme catalytic centre.<sup>[2]</sup> Much of our knowledge of the catalytic cycle of these enzymes is derived from the first structurally characterised cytochrome P450, P450<sub>cam</sub>, a stereoselective camphor hydroxylating enzyme from a *Pseudomonas* bacterium.<sup>[3]</sup> The X-ray crystal structures of many P450s from

across a variety of different species have now been determined.<sup>[4]</sup>

The structures of the ligand-bound (substrate and inhibitors) and substrate-free P450 enzymes are accessible through X-ray crystallography. The remaining intermediates of the P450 catalytic cycle can be explored using other techniques.<sup>[5]</sup> X-ray crystallographic structures of certain intermediates of P450 enzymes have been proposed but these species are challenging to isolate in the multi-step catalytic cycle of these enzymes. For other enzymes the use of cryogenic temperatures and rapid-data collection techniques have enabled the trapping and characterisation of intermediates in enzyme-catalysed reactions in crystallo.<sup>[6]</sup> One major challenge is initiating the reaction in P450 enzymes. This is hampered by the need for external electron transfer partners and nicotinamide cofactors (NAD(P)H) to initiate reactions.<sup>[7]</sup> Others have attempted to overcome this by reducing a crystal of substrate-bound P450s with electrons from the X-ray beam and in certain instances this can result in substrate oxidation.<sup>[8]</sup> A cryoreduction approach resulted in formation of electron density above the heme that was proposed to be consistent with an oxyferryl (Cpd I), the main oxidant of the P450 catalytic cycle.<sup>[9]</sup> Cryoreduction of such high oxidation state intermediates and ferric heme is now recognised to be problematic. Cpd I is proposed to only be definitively trapped and characterised by spectroscopic methods, though cryoradiolysis experiments on crystals can generate product.<sup>[5a]</sup>

An alternate strategy to initiating enzymatic reactions in protein crystals of P450 enzymes is the use of the peroxide shunt pathway.<sup>[10]</sup> The peroxide shunt pathway is able to generate Cpd I (Scheme 1) directly using hydrogen peroxide. A small number of P450s are able to use this pathway for catalysis to act as peroxxygenases.<sup>[11]</sup> As this shunt pathway and these P450 peroxxygenases only require hydrogen peroxide (H<sub>2</sub>O<sub>2</sub>) to

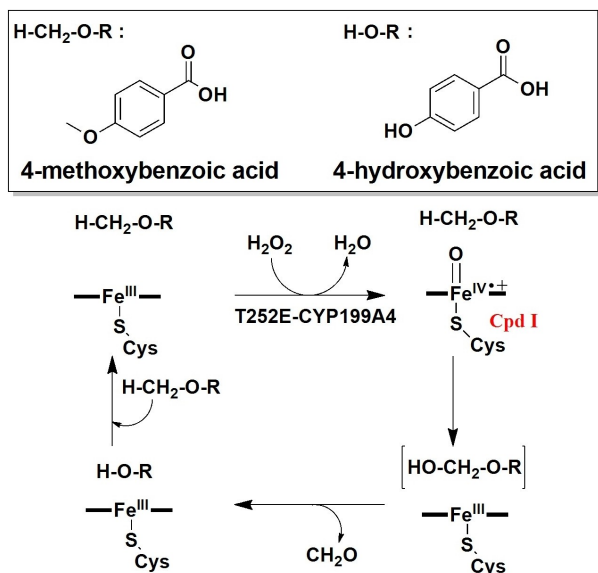
[a] Dr. J. H. Z. Lee, Dr. S. G. Bell  
Department of Chemistry  
University of Adelaide  
Adelaide, SA 5005 (Australia)  
E-mail: stephen.bell@adelaide.edu.au

[b] Dr. J. B. Bruning  
School of Biological Sciences  
University of Adelaide  
Adelaide, SA 5005 (Australia)

[\*\*] A previous version of this manuscript has been deposited on a preprint server (<https://doi.org/10.26434/chemrxiv-2023-xmhgz>).

Supporting information for this article is available on the WWW under <https://doi.org/10.1002/chem.202303335>

© 2023 The Authors. Chemistry - A European Journal published by Wiley-VCH GmbH. This is an open access article under the terms of the Creative Commons Attribution Non-Commercial License, which permits use, distribution and reproduction in any medium, provided the original work is properly cited and is not used for commercial purposes.



**Scheme 1.** The O-demethylation of 4-methoxybenzoic acid catalysed by the peroxide shunt pathway of T252E-CYP199A4 using H<sub>2</sub>O<sub>2</sub>.

initiate reactions, it may be possible to trigger in crystallo P450 reactions by simply soaking the crystal with peroxide. This could be used to obtain product bound structures. In principle, with the appropriate techniques and equipment for example, free electron laser sources, there would also be the potential to trap and study the reactive intermediates involved in these enzyme reactions.<sup>[12]</sup>

An attempt at capturing an in crystallo P450 enzyme reaction using hydrogen peroxide has been described previously.<sup>[13]</sup> A weak region of electron density was observed in the X-ray crystal structure of substrate-bound crystals of the P450 enzyme CYP121 after soaking with H<sub>2</sub>O<sub>2</sub> and was proposed to correspond to a hydroxylated hemiacetal intermediate. A study with a peroxiredoxin enzyme also exploited a similar method to initiate in crystallo enzymatic reactions. Crystals of peroxiredoxin were soaked with H<sub>2</sub>O<sub>2</sub> and structures were solved. Atomic resolution snapshots of the peroxiredoxin proceeding through thiolate, sulfenate, and sulfinate species were obtained.<sup>[14]</sup> Crystal soaking experiments with H<sub>2</sub>O<sub>2</sub> have been reported with other heme enzymes, including lactoperoxidase and chloroperoxidase, that contain electron density of peroxide trapped within the crystallised protein enabling the characterisation of reactive intermediates.<sup>[15]</sup> Despite these studies, efficient activation of heme-dependent oxygenases within crystals remains a challenge and new methods are required to achieve this.

CYP199A4 is a bacterial P450 enzyme from the bacterium *Rhodospseudomonas palustris* HaA2 that has high catalytic activity towards the oxidation of *para*-substituted benzoic acids.<sup>[16]</sup> The structure of CYP199A4 has been studied by X-ray crystallography to elucidate the binding modes of various ligands and rationalise the activity of this P450 enzyme.<sup>[17]</sup> CYP199A4 and its mutants have also been used as a model system to investigate mechanistic details of P450 reactions.<sup>[17d,18]</sup>

A variant of CYP199A4, the T252E mutant (T252E-CYP199A4), was found to shut down monooxygenase activity and to have enhanced peroxygenase activity using only H<sub>2</sub>O<sub>2</sub> to support catalytic activity.<sup>[18b,19]</sup> This method has also been demonstrated to work with other P450 enzymes.<sup>[11g,20]</sup> A crystal structure of T252E-CYP199A4 complexed with 4-methoxybenzoic acid has been solved.<sup>[19]</sup> Given the enhanced peroxygenase activity of this P450 variant with turnovers numbers in excess of 100, we hypothesise it should be capable of in crystallo enzymatic reactions using hydrogen peroxide. By soaking crystals of T252E-CYP199A4 bound to 4-methoxybenzoic acid with H<sub>2</sub>O<sub>2</sub>, we aim to assess if peroxygenase activity to oxidatively O-demethylate this substrate could occur within these crystals (Scheme 1).<sup>[19]</sup>

## Results

For in crystallo enzymatic reactions with T252E-CYP199A4, 4-methoxybenzoic acid was chosen as the substrate as it binds to both the WT and T252E-CYP199A4 ( $K_d = 0.3 \mu\text{M}$  and  $1.1 \mu\text{M}$ , respectively).<sup>[16b,19]</sup> Diffraction data of T252E-CYP199A4 co-crystallised with 4-hydroxybenzoic acid was first collected to enable comparison to the H<sub>2</sub>O<sub>2</sub>-soaked crystals to both the substrate-bound (PDB 7REH) and product-bound structures.

The structure of T252E-CYP199A4 co-crystallised with 4-hydroxybenzoic acid was solved and refined to a resolution of  $2.03 \text{ \AA}$  (PDB: 8GLY, Table S1). The overall protein fold was similar to the structure of T252E-CYP199A4 (PDB: 7REH, RMSD of  $0.157 \text{ \AA}$ , Figure S1).<sup>[19]</sup> There was electron density consistent with the mutated T252E residue and the retention of the 6<sup>th</sup> aqua ligand of the heme as observed with other T252E-CYP199A4 crystal structures (Figure 1).<sup>[18b,19]</sup> There was also electron density present within the active site consistent with a bound product ligand.<sup>[21]</sup> This electron density was modelled as 4-hydroxybenzoic acid (occupancy 86%). The overall active site structure was similar to that of the substrate-bound structure with little or no differences observed between the positioning of key active site residues (Figure S2).

When the ligand was modelled as 4-methoxybenzoic acid (Figure 1), there was a distinct region of negative density where the methoxy functional group would be. This negative density clearly demonstrates that the additional atoms of 4-methoxybenzoic acid are a poor fit for the electron density of the 4-hydroxybenzoic acid product. A similar analysis was carried with T252E-CYP199A4 co-crystallised with 4-methoxybenzoic acid but modelled with 4-hydroxybenzoic acid (Figure S3). This demonstration of the difference in the  $F_o - F_c$  maps between the substrate ligand and the electron density of the product would assist in determining if the H<sub>2</sub>O<sub>2</sub>-soaked crystals of T252E-CYP199A4 underwent O-demethylation.

Protein crystals of T252E-CYP199A4 complexed with 4-methoxybenzoic acid were soaked with different concentrations of H<sub>2</sub>O<sub>2</sub> to trigger the in crystallo reaction ( $0.5\text{--}10 \text{ mM H}_2\text{O}_2$  for  $\sim 10 \text{ s--}10 \text{ min}$ ). A total of 24 crystals of the T252E mutant were soaked in varying concentrations of H<sub>2</sub>O<sub>2</sub> for different lengths of time and then cryo-cooled in liquid N<sub>2</sub>. X-ray diffraction data

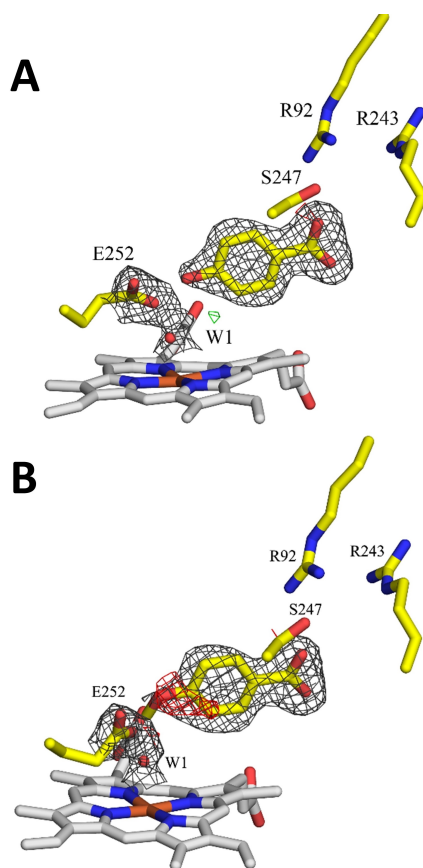


**Figure 1.** Crystal structure of T252E-CYP199A4 co-crystallised with 4-hydroxybenzoic acid (yellow sticks, PDB: 8GLY). In (A), the electron density of the bound substrate was modelled as 4-hydroxybenzoic acid and in (B) it was modelled as 4-methoxybenzoic acid. Composite-omit maps ( $2mF_o - F_c$ ) are shown as a grey mesh contoured to  $1.0 \sigma$  ( $1.5 \text{ \AA}$  carve) around the substrate, residue E252 and heme-bound water in (A) and (B).  $F_o - F_c$  maps contoured to  $2.5 \sigma$  are also shown as a green (positive density) or red (negative density) mesh. In (B), there is a region of negative density around where the methoxy functional group would be located.

were collected. Three of these crystals showed high quality diffraction patterns. The structures of these crystals were determined and refined (Figures 2, S4–S6, and Table S1). The  $F_o - F_c$  difference maps were generated to assess negative and positive electron density around the bound molecule and confirm if in crystallo demethylation to generate 4-hydroxybenzoic acid occurred.

The first structure solved for the in crystallo reactions was a crystal soaked with 1 mM  $\text{H}_2\text{O}_2$  and cryo-cooled immediately after addition of the peroxide ( $\leq 10 \text{ s}$ , henceforth abbreviated as 0 min). This structure was solved and refined to a resolution of  $1.85 \text{ \AA}$  (PDB: 8GM1; Figures 2 and S7). When comparing the  $F_o - F_c$  maps between the two models, the 4-hydroxybenzoic acid model showed a large region of positive density (green mesh) surrounding the *para*-hydroxy moiety indicating the model used is missing atoms in this region (Figure 2). In the 4-methoxybenzoic acid model (Figure 2), no positive or negative density was observed near the *para* position of the bound ligand. This demonstrates that little or no demethylation of 4-

methoxybenzoic acid had occurred within the crystal (Figure S7 and Figure S8).

The other structures were from crystals soaked in  $\text{H}_2\text{O}_2$  for longer. In the crystal structure of T252E-CYP199A4 with 4-methoxybenzoic acid that was soaked with 4 mM of  $\text{H}_2\text{O}_2$  for 5 min, the  $F_o - F_c$  maps showed only a small region of positive density near the *para*-moiety when 4-hydroxybenzoic acid is the modelled ligand (resolution of  $2.02 \text{ \AA}$ ; PDB: 8GLZ; Figures 2 and S9). In the and 4-methoxybenzoic acid model there was negative density around the *para*-methoxy moiety that indicates poor agreement between this model and the electron density (Figures 2 and S9). For this structure, the  $F_o - F_c$  and composite-omit maps were similar to that of T252E-CYP199A4 bound to 4-hydroxybenzoic acid (Figure 1). Taken together this is strong evidence of 4-hydroxybenzoic acid bound within the active site and that an in crystallo demethylation reaction has occurred. The positive density surrounding the 4-hydroxybenzoic acid model (Figure S9) is also significantly smaller in comparison to the crystal where little or no demethylation of the substrate occurred (Figure S7).

The crystal structure of T252E-CYP199A4 bound to 4-methoxybenzoic acid that was soaked in 2 mM  $\text{H}_2\text{O}_2$  for 10 min was determined at  $2.33 \text{ \AA}$  resolution (PDB: 8GM2; Table S1, Figures 2 and S10). The model of both 4-hydroxybenzoic acid and 4-methoxybenzoic acid showed no significant regions of negative density. However, a small region of positive density was observed with the 4-hydroxybenzoic acid model (Figure 2) indicative that some proportion of the 4-methoxybenzoic acid ligand has undergone O-demethylation within this crystal.

Modelling the electron density of the ligands bound to the different  $\text{H}_2\text{O}_2$ -soaked crystals with either 4-methoxybenzoic acid or 4-hydroxybenzoic acid suggests that different proportions of the initial substrate and demethylated metabolite were present in the T252E-CYP199A4 crystals. To further investigate the extent of the progress of the in crystallo enzymatic reaction, both 4-methoxybenzoic acid and 4-hydroxybenzoic acid were modelled in same location (Table 1, Figure S11). The refined occupancies of the bound ligand to the soaked crystals were largely consistent with what was observed with the  $F_o - F_c$  maps (Figure 2). The 4 mM  $\text{H}_2\text{O}_2$ -soaked crystal showed the highest

**Table 1.** Occupancies of 4-methoxybenzoic acid and 4-hydroxybenzoic acid co-refined at the same location in  $\text{H}_2\text{O}_2$  soaked crystals of T252E-CYP199A4.

| Condition                                       | Ligand occupancy [%] |             |
|---|----------------------|-------------|
|   | 4-hydroxyBA          | 4-methoxyBA |
| 4 mM $\text{H}_2\text{O}_2$ /5 min (PDB: 8GLZ)  | 70                   | 30          |
| 2 mM $\text{H}_2\text{O}_2$ /10 min (PDB: 8GM2) | 35                   | 62          |
| 1 mM $\text{H}_2\text{O}_2$ /0 min (PDB: 8GM1)  | 47                   | 50          |
| 4-hydroxyBA (PDB: 8GLY)                         | 86                   | –           |
| 4-methoxyBA (PDB: 7REH)                         | –                    | 100         |

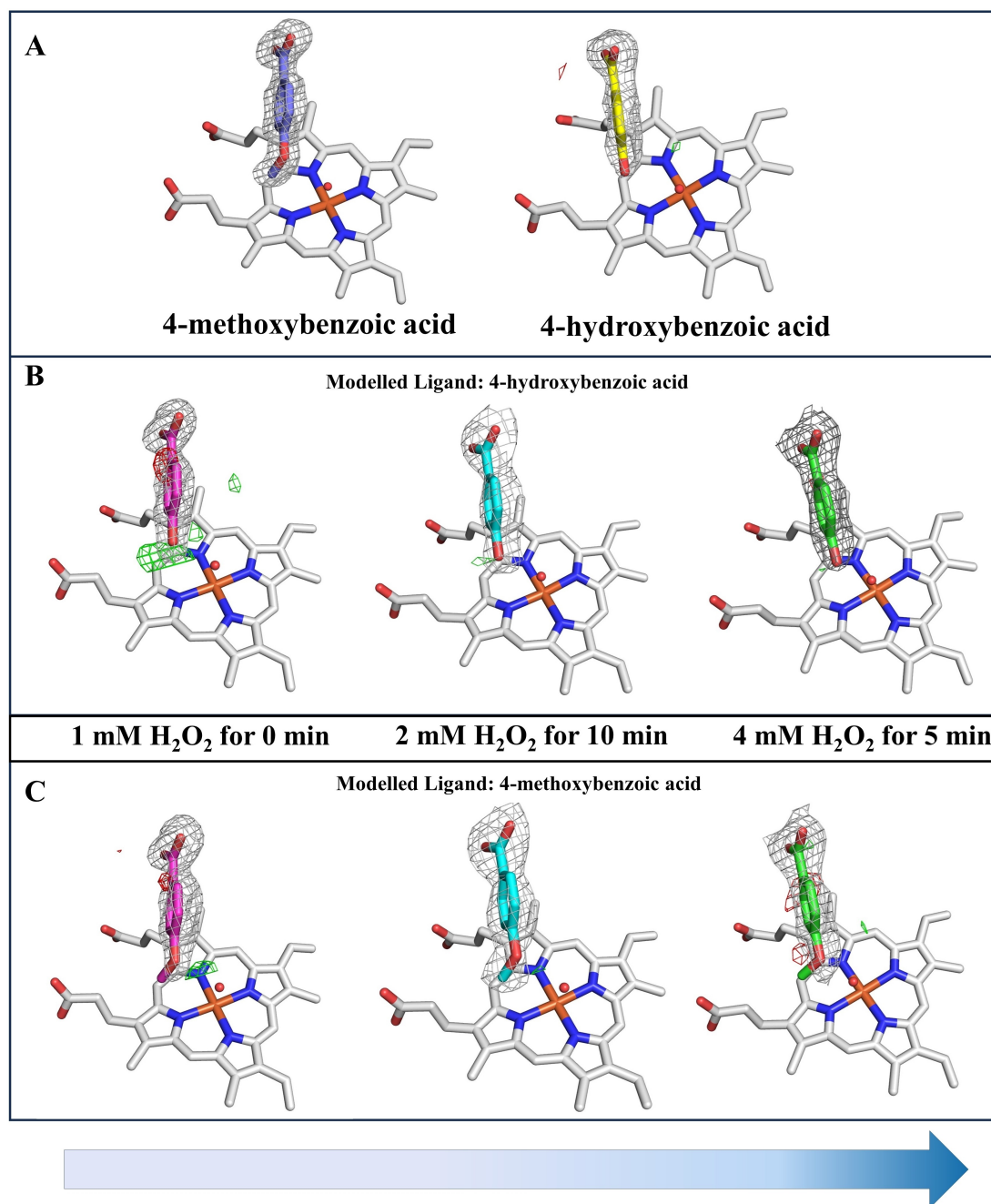


**Figure 2.** (A) Crystal structure of T252E-CYP199A4 co-crystallised with 4-methoxybenzoic acid (PDB: 7REH) and 4-hydroxybenzoic acid (PDB: 8GLY) highlighting the electron density of the ligand in each structure. (B) Crystal structures of the three crystals of T252E-CYP199A4 co-crystallised with 4-methoxybenzoic acid as substrate and soaked with H<sub>2</sub>O<sub>2</sub> for different time periods (PDB: 8GLZ, 8GM2, 8GM1). In (B), the electron density within the active site of these structures was modelled as 4-hydroxybenzoic acid, which was the expected product of *in crystallo* demethylation of the substrate. (C) The same crystals as in (B) but the electron density within the active site was modelled as the 4-methoxybenzoic acid substrate instead. Composite-omit maps ( $2mF_o - F_c$ ) are shown as a grey mesh contoured to 1.0  $\sigma$  (1.5 Å carve) around the ligand.  $F_o - F_c$  maps contoured to 2.5  $\sigma$  are also shown as a green (positive electron density) or red (negative electron density) mesh. Comparing the difference in  $F_o - F_c$  maps between the two modelled ligands across the three structures indicated that the greatest degree of *in crystallo* demethylation occurred in the crystal soaked with 4 mM H<sub>2</sub>O<sub>2</sub> for 5 min.

proportion of 4-hydroxybenzoic acid (70%, Table 1). Crystals soaked with 1 mM and 2 mM H<sub>2</sub>O<sub>2</sub> showed less or no *in crystallo* demethylation occurring based on the  $F_o - F_c$  maps (Figures 2 and 4). The occupancy of 4-methoxybenzoic acid for

these two crystals was higher compared to the demethylated product (Table 1).

The exposure of peroxide to P450 enzymes such as T252E-CYP199A4 and other P450 peroxxygenases has been shown to damage the heme centre.<sup>[18b,19,22]</sup> To assess if this peroxide-



driven damage causes any changes with the  $\text{H}_2\text{O}_2$ -soaked crystals the crystals that were soaked with 4 mM  $\text{H}_2\text{O}_2$  and 2 mM  $\text{H}_2\text{O}_2$  for 5 min and 10 min respectively were modelled with their respective ligand with the highest refined occupancy in Table 1. Their active site structure of each crystal was compared to a structure of T252E-CYP199A4 bound to 4-methoxybenzoic acid (PDB: 7REH) and T252E-CYP199A4 with 4-hydroxybenzoic acid (PDB: 8GLY; Figures 3, S12–S13). The distances and angles of key active site features for these crystal structures were measured and compared (Table S2). The general features of the active site across all the structures were similar. The chloride capping anion (Figure 3) is present alongside the water molecules that interact with the heme and benzoic acid moiety of the ligand.<sup>[16a]</sup> There was no evidence of heme damage that would infer peroxide induced heme damage (Figures 4 and S12).<sup>[19]</sup>

The active site structure of the  $\text{H}_2\text{O}_2$ -soaked crystals of T252E-CYP199A4 also showed no significant differences with the previously reported structure of this enzyme (Figure 3, PDB: 7REH). In the crystal structure of T252E-CYP199A4 soaked with

2 mM  $\text{H}_2\text{O}_2$  for 10 min (2.33 Å, PDB: 8GM2) an altered conformation for the mutated E252 residue was observed in the  $\text{H}_2\text{O}_2$  soaked crystal (Figure 4B and Figure S13). The carboxylate of the E252 residue was oriented upwards by  $\sim 18^\circ$  after soaking with  $\text{H}_2\text{O}_2$  and was more parallel with the plane of the heme (Figure S13).

In summary, three different crystals of T252E-CYP199A4 in complex with 4-methoxybenzoic acid were soaked in varying concentrations of  $\text{H}_2\text{O}_2$  (Figure 4). The crystal of the T252E mutant soaked for 4 mM  $\text{H}_2\text{O}_2$  for 5 min showed a loss of electron density of the bound ligand that was consistent with in crystallo *O*-demethylation.

## Discussion

The structure of T252E-CYP199A4 in complex with 4-hydroxybenzoic acid has been solved. This ligand is a product of *O*-demethylation by CYP199A4 using 4-methoxybenzoic acid as a substrate. 4-Methoxybenzoic acid binds to WT CYP199A4 with submicromolar affinity ( $K_d = 0.3 \mu\text{M}$ )<sup>[16b]</sup> and the T252E mutant ( $K_d = 1.1 \mu\text{M}$ )<sup>[19]</sup> The binding affinity of 4-hydroxybenzoic acid would be expected to be lower. For example, the dissociation constants for P450<sub>cam</sub> with its physiological substrate, camphor ( $K_d = 0.25 \mu\text{M}$ )<sup>[23]</sup> showed it was bound nearly 40-fold tighter compared to the product, 5-*exo*-hydroxycamphor ( $K_d = \sim 10 \mu\text{M}$ ).<sup>[24]</sup> The refined occupancy of 4-hydroxybenzoic acid

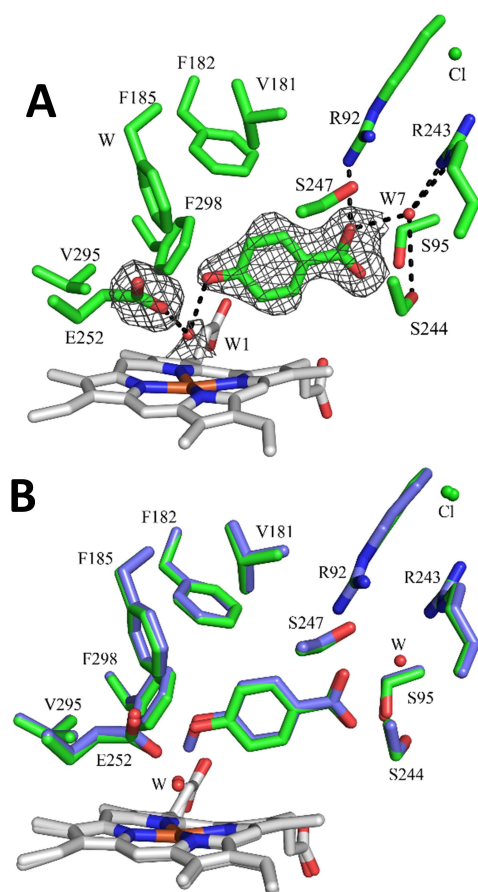


**Figure 3.** (A) The structure of T252E-CYP199A4 crystallised with 4-methoxybenzoic acid solved to 2.02 Å that underwent in crystallo demethylation after soaking with 4 mM  $\text{H}_2\text{O}_2$  for 5 min (green sticks, PDB: 8GLZ). The ligand bound was modelled as 4-hydroxybenzoic acid. A composite-omit map ( $2mF_o - F_c$ ) is shown around the bound ligand, residue E252 and heme-bound water (W1) as a grey mesh (1.0  $\sigma$ , 1.5 Å carve). (B) Structure of T252E-CYP199A4 soaked with 4 mM  $\text{H}_2\text{O}_2$  (green sticks) superimposed with the same enzyme complexed with 4-methoxybenzoic acid (navy sticks, PDB: 7REH).

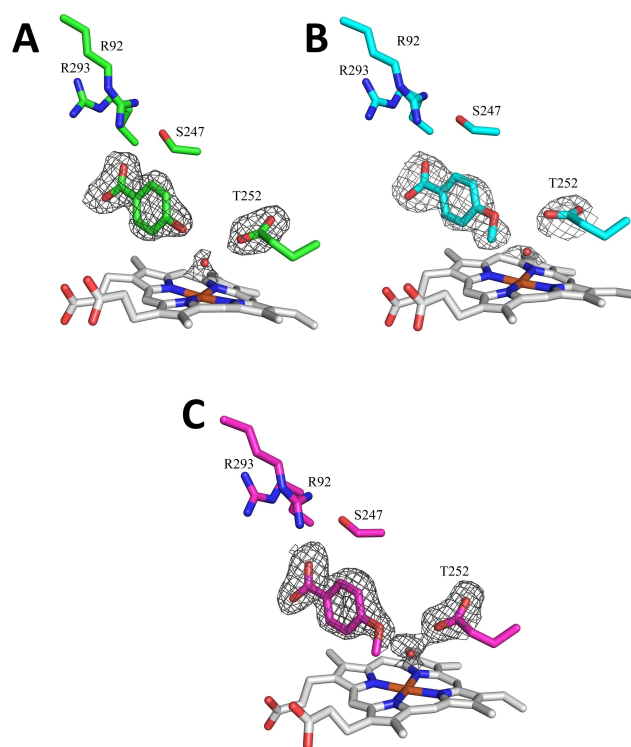


**Figure 4.** Crystal structures of T252E-CYP199A4 soaked with  $\text{H}_2\text{O}_2$ . In (A), crystal was soaked with 4 mM  $\text{H}_2\text{O}_2$  for 5 min and 4-hydroxybenzoic acid was the highest occupancy ligand observed. In (B) and (C), crystals were soaked with 2 mM and 1 mM  $\text{H}_2\text{O}_2$  respectively while 4-methoxybenzoic acid was the highest occupancy ligand observed for both (B) and (C). Composite omit maps are shown as a grey mesh (1.0  $\sigma$ , 1.5 Å carve).

bound to T252E-CYP199A4 was found to be 86%. The ligand binding mode and active site geometry of T252E-CYP199A4 was not altered significantly with 4-hydroxybenzoic acid compared to 4-methoxybenzoic acid. A structure of P450<sub>cam</sub> bound to the hydroxylation product, 5-exo-hydroxycamphor found the product and substrate are held in similar positions.<sup>[3b]</sup>

The structure of P450<sub>cam</sub> with 5-exo-hydroxycamphor also revealed an interaction between the product OH group and the heme-iron centre (Fe–O,  $\approx 2.7$  Å). The alcohol group of 4-hydroxybenzoic acid was further away from the iron (Fe–O, 4.8 Å) and interacts with a heme-bound distal water ligand (83% occupancy). This was to be expected as other benzoic acid substrates were also unable to displace this heme-bound water in this mutant.<sup>[19]</sup> This is due to the distal water molecule interacting with the carboxylate of E252 (2.6 Å) and allows it to remain bound to the heme-iron.

In crystallo *O*-demethylation reactions were demonstrated with crystallised T252E-CYP199A4 bound to 4-methoxybenzoic acid and soaked with H<sub>2</sub>O<sub>2</sub>. The soaking condition that drove demethylation to the greatest degree (70%) being 4 mM H<sub>2</sub>O<sub>2</sub> for 5 min and this was the highest concentration of H<sub>2</sub>O<sub>2</sub> tested. The other soaking conditions using lower amounts of H<sub>2</sub>O<sub>2</sub> were less successful. Differences in the level of *O*-demethylation could be due to poorer diffusion of H<sub>2</sub>O<sub>2</sub> into and through the crystal lattice. The rate of diffusion depends on a number of factors including the crystals size and diffusion coefficients.<sup>[25]</sup> The use of smaller crystals may be advantageous. The sizes of the crystals chosen for this initial study were chosen at random. Crystals with edge lengths in single digit  $\mu\text{m}$  or smaller are recommended for diffusion triggered in crystallo reactions.<sup>[25]</sup>

Large-scale batch crystallisation to form microcrystals of the desired P450 peroxygenase could be achieved by incorporating ammonium sulfate precipitation to the vapor diffusion crystallisation method.<sup>[26]</sup> Protein microcrystals are susceptible to damage to X-ray radiation,<sup>[25]</sup> but large batches of them can be used for serial crystallography using X-ray free electron lasers (XFEL).<sup>[12d]</sup> As diffraction is essentially instantaneous in serial crystallography this method could obtain diffraction data to explore femtosecond resolved structures along the catalytic pathway of enzymes.

Smaller crystals with large diffusion coefficients would allow fast diffusion of the target molecule into the crystal lattice and is influenced by large, water-filled channels within the crystallised protein.<sup>[25]</sup> The size of the solvent pores within crystals of CYP199A4 has not been assessed. A possible approach to improve the diffusion of H<sub>2</sub>O<sub>2</sub> into the crystals of this P450 enzyme would be analysing the solvent channels of the enzyme using CAVER 3.0.<sup>[27,28]</sup> For example, this method was used to identify and estimate the importance of the solvent channels in haloalkane dehalogenase DhaA for catalytic activity.<sup>[27]</sup>

In crystallo P450 reactions driven by the peroxide shunt has only been demonstrated with CYP121 with a synthetic probe designed to mimic its native substrate, cyclo(I-Tyr-I-Tyr) (cYY).<sup>[13]</sup> Soaking of CYP121 co-crystallised with the synthetic probe in H<sub>2</sub>O<sub>2</sub> was reported to form a hydroxylated intermediate (Figure S14). This normally unstable hemiacetal intermediate was reported to share 50% occupancy with the substrate precursor.

This was less clear when these changes in the electron density were compared to those observed in this work (Figure S13 and Figure 2). Other substrates could be crystallised T252E-CYP199A4 to assess different in crystallo P450 reactions such as hydroxylation and sulfoxidation. It is envisioned that trapping H<sub>2</sub>O<sub>2</sub> within the crystallised enzyme could be achieved to assess how the peroxide molecule interacts with the heme and active site residues as has been demonstrated with diiron hydroxylases.<sup>[29]</sup> While this paper was being revised a report of using serial crystallography at an X-ray free electron lasers facility demonstrating the trapping of a ferric-hydroperoxo intermediate.<sup>[30]</sup>

## Conclusions

In summary, a crystal structure of T252E-CYP199A4 complexed with 4-hydroxybenzoic acid was solved. Active site geometry and ligand binding modes of enzyme complex did not differ significantly from when the enzyme was bound to 4-methoxybenzoic acid. In crystallo *O*-demethylation of 4-methoxybenzoic acid was conclusively demonstrated within crystals of T252E-CYP199A4.

## Materials and Methods

General reagents and organics were purchased from Sigma-Aldrich. Isopropyl- $\beta$ -D-thiogalactopyranoside (IPTG) and buffer components were obtained from Astral Scientific (Australia). UV/Vis spectra and spectroscopic activity assays were performed on an Agilent Cary 60 spectrophotometer at  $30 \pm 5^\circ\text{C}$ .

**Production and purification of T252E-CYP199A4:** Mutant T252E of CYP199A4 was expressed as previously described but with the addition of 4-methoxybenzoic acid to a concentration of 1 mM to the expression media before induction. The expressed protein was then purified using previously established methods.<sup>[19]</sup> Proteins were stored in 50% v/v glycerol at  $-20^\circ\text{C}$ .

**Protein crystallography and in crystallo enzymatic reactions:** Crystallisation experiments were performed with T252E-CYP199A4. Immediately prior to preparation of crystal trays, the protein was purified via elution through a HiPrep Sephacryl S-200 HR size-exclusion column (60 cm $\times$ 16 mm; GE Healthcare) with Buffer T at a flow rate of 1 mL min<sup>-1</sup>. The purity of the protein was assessed based on the Reinheitszahl value,  $RZ = A_{420}/A_{280}$ , whereby fractions with  $RZ = 2$  were collected and combined.

The ligands (4-methoxy- or 4-hydroxy-benzoic acid) in DMSO were then added to the combined fractions to a final concentration of 1 mM from a 100 mM stock to the concentrated protein. The combined fractions with substrate were incubated at  $4^\circ\text{C}$  and then concentrated via ultrafiltration using a Microsep Advance centrifugal device (10 kDa MWCO, Pall Corporation) to a concentration of approximately 30–35 mg mL<sup>-1</sup>. Crystallisation trays were prepared using the following optimised buffer conditions previously reported: 0.2 M magnesium acetate, 100 mM Bis-Tris buffer (adjusted with acetic acid to pH 5.0–5.75) and 20–32% w/v polyethylene glycol (PEG) 3350.<sup>[21]</sup> Protein crystallisation was achieved using the hanging-drop vapor diffusion method in 24-well trays. An equal volume of crystallisation buffer was mixed with hanging drops of 1.2–2  $\mu\text{L}$  of protein and was equilibrated with a reservoir of the

same buffer (500  $\mu$ L) at 16 °C. Red plate-like crystals were obtained after half a day to one week.

In crystallo reactions were carried out with T252E-CYP199A4 co-crystallised with 4-methoxybenzoic acid. Single crystals were picked from individual wells and soaked in their respective crystallisation buffer containing  $\text{H}_2\text{O}_2$ . The crystals were soaked at different concentrations of  $\text{H}_2\text{O}_2$  (0.5 to 10 mM) with variable soaking times (0, 5 and 10 min). After soaking, single crystals were mounted onto Micromounts or Microloops (MiTeGen LLC, New York, USA). Mounted crystals were immersed in Parabar 10312 Oil (Paratone-N, Hampton Research, California, USA) before flash-cooled in liquid  $\text{N}_2$ .

X-ray diffraction data were obtained (360 images per crystal) at the Australian Synchrotron using the MX1 beamline<sup>[31]</sup> with an exposure time of 1 s, oscillation angle of 1°, wavelength of 0.9537 Å and temperature of 100 K. Diffraction images were indexed and integrated using iMosfilm.<sup>[32]</sup> Aimless<sup>[33]</sup> from the CCP<sub>4</sub> suite of programs<sup>[34]</sup> was used to carry out scaling, merging and  $R_{\text{free}}$  labelling (5% of reflections, randomly selected). The phase problem was solved using Molecular Replacement in Phaser<sup>[35]</sup> using a high-resolution structure of WT CYP199A4 (1.54 Å, PDB: 5UVB) as the search model. The ligands and solvent molecules were removed from the search model prior to phasing to eliminate model bias. Weighted  $2mF_o - F_c$  maps and  $F_o - F_c$  difference maps were obtained and used to rebuild the model in WinCoot and determine the substrate binding mode.<sup>[36]</sup> In addition to modelling individual ligand both 4-methoxybenzoic acid and 4-hydroxybenzoic acid were modelled in same location using different alternative location (altloc) identifiers and the occupancies of both ligands refined. Structural refinements were carried out over multiple cycles using Phenix Refine, available in the Phenix suite of programs.<sup>[37]</sup> Refinement statistics are shown in Table S1.

Composite-omit or feature enhanced maps that reduce model bias were generated in Phenix to allow inspection of the ligand binding site and reveal the location of all substrate atoms.<sup>[38]</sup> Detailed data collection and structural refinement statistics are provided in the Supporting Information. To model the location of the Cpd I oxygen atom (Table S2), the CreateAtomAlongBond script was employed. Computational studies of Cpd I have calculated that the Fe–O bond length is very consistent at 1.62 Å. This was determined both in the absence and in the presence of substrate for CYPs 2C9, 2D6, 3A4 and P450<sub>cam</sub>.<sup>[39]</sup> The oxygen atom was thus positioned 1.62 Å from the heme iron of the CYP199A4 structures.

## Acknowledgements

The authors acknowledge the Australian Government for Research Training Program Scholarships (PhD to JHZL). JHZL thanks the University of Adelaide for a Constance Fraser PhD Scholarship and the CSIRO Synthetic Biology Future Science Platform for a PhD top-up Scholarship. We would like to thank the scientists at the MX1 beamline at the Australian Synchrotron for help with data collection. We acknowledge ANSTO for financial support and in providing the facility used in this work. The authors thank Dr Tom Coleman for a photo of crystallised CYP199A4. Open Access publishing facilitated by The University of Adelaide, as part of the Wiley - The University of Adelaide agreement via the Council of Australian University Librarians.

## Conflict of Interests

The authors declare no conflict of interest.

## Data Availability Statement

The data that support the findings of this study are available in the supplementary material of this article.

**Keywords:** cytochrome P450s · heme enzymes · In crystallo reactions · peroxygenases · X-ray crystallography

- [1] F. P. Guengerich, *J. Biol. Chem.* **2013**, 288, 17063–17064.
- [2] a) D. Sirim, F. Wagner, A. Lisitsa, J. Pleiss, *BMC Biochem.* **2009**, 10; b) D. Sirim, M. Widmann, F. Wagner, J. Pleiss, *BMC Struct. Biol.* **2010**, 10.
- [3] a) T. L. Poulos, B. C. Finzel, I. C. Gunsalus, G. C. Wagner, J. Kraut, *J. Biol. Chem.* **1985**, 260, 16122–16130; b) H. Li, S. Narasimulu, L. M. Havran, J. D. Winkler, T. L. Poulos, *J. Am. Chem. Soc.* **1995**, 117, 6297–6299; c) T. L. Poulos, B. C. Finzel, A. J. Howard, *Biochemistry (Mosc.)* **1986**, 25, 5314–5322; d) R. Raag, T. L. Poulos, *Biochemistry (Mosc.)* **1989**, 28, 7586–7592.
- [4] a) T. L. Poulos, E. F. Johnson, in *Cytochrome P450 Structure, Mechanism, and Biochemistry*, (Ed.: P. R. Ortiz de Montellano), Springer US, **2005**, pp. 87–114; b) T. L. Poulos, E. F. Johnson, in *Cytochrome P450*, Springer International Publishing, **2015**, pp. 3–32; c) T. L. Poulos, A. H. Follmer, *Acc. Chem. Res.* **2022**, 55, 373–380; d) I. G. Denisov, T. M. Makris, S. G. Sligar, I. Schlichting, *Chem. Rev.* **2005**, 105, 2253–2278.
- [5] a) J. Rittle, M. T. Green, *Science* **2010**, 330, 933–937; b) P. J. Mak, I. G. Denisov, *Biochim. Biophys. Acta Proteins Proteomics* **2018**, 1866, 178–204.
- [6] B. L. Stoddard, *Pharmacol. Ther.* **1996**, 70, 215–256.
- [7] I. Schlichting, R. S. Goody, in *Methods in Enzymology*, Elsevier, **1997**, pp. 467–490.
- [8] a) V. C. Murarka, D. Batabyal, J. A. Amaya, I. F. Sevrioukova, T. L. Poulos, *Biochemistry* **2020**, 59, 2743–2750; b) D. Batabyal, T. L. Poulos, *Biochemistry* **2013**, 52, 8898–8906; c) S. Tripathi, H. Li, T. L. Poulos, *Science* **2013**, 340, 1227–1230.
- [9] I. Schlichting, J. Berendzen, K. Chu, A. M. Stock, S. A. Maves, D. E. Benson, R. M. Sweet, D. Ringe, G. A. Petsko, S. G. Sligar, *Science* **2000**, 287, 1615–1622.
- [10] a) E. G. Hrycay, S. M. Bandiera, in *Monooxygenase, Peroxidase and Peroxygenase Properties and Mechanisms of Cytochrome P450*, Springer International Publishing, **2015**, pp. 1–61; b) A. W. Munro, K. J. McLean, J. L. Grant, T. M. Makris, *Biochem. Soc. Trans.* **2018**, 46, 183–196.
- [11] a) I. Matsunaga, M. Yamada, E. Kusunose, Y. Nishiuchi, I. Yano, K. Ichihara, *FEBS Lett.* **1996**, 386, 252–254; b) A. C. Harlington, K. E. Shearwin, S. G. Bell, F. Whelan, *Chem. Commun.* **2022**, 58, 13321–13324; c) O. Shoji, C. Wiese, T. Fujishiro, C. Shirataki, B. Wunsch, Y. Watanabe, *J. Biol. Inorg. Chem.* **2010**, 15, 1109–1115; d) T. Fujishiro, O. Shoji, S. Nagano, H. Sugimoto, Y. Shiro, Y. Watanabe, *J. Biol. Chem.* **2011**, 286, 29941–29950; e) H. Onoda, S. Tanaka, Y. Watanabe, O. Shoji, *Faraday Discuss.* **2022**, 234, 304–314; f) O. Shoji, Y. Watanabe, *J. Biol. Inorg. Chem.* **2014**, 19, 529–539; g) O. Shoji, T. Fujishiro, K. Nishio, Y. Kano, H. Kimoto, S.-C. Chien, H. Onoda, A. Muramatsu, S. Tanaka, A. Hori, H. Sugimoto, Y. Shiro, Y. Watanabe, *Catal. Sci. Technol.* **2016**, 6, 5806–5811; h) H. Onoda, O. Shoji, K. Suzuki, H. Sugimoto, Y. Shiro, Y. Watanabe, *Catal. Sci. Technol.* **2018**, 8, 434–442.
- [12] a) C. Kupitz, J. L. Olmos, Jr., M. Holl, L. Tremblay, K. Pande, S. Pandey, D. Oberthür, M. Hunter, M. Liang, A. Aquila, J. Tenboer, G. Calvey, A. Katz, Y. Chen, M. O. Wiedorn, J. Knoska, A. Meents, V. Majriani, T. Norwood, I. Poudyal, T. Grant, M. D. Miller, W. Xu, A. Tolstikova, A. Morgan, M. Metz, J. M. Martin-Garcia, J. D. Zook, S. Roy-Chowdhury, J. Coe, N. Nagaratnam, D. Meza, R. Fromme, S. Basu, M. Frank, T. White, A. Barty, S. Bajt, O. Yefanov, H. N. Chapman, N. Zatsepin, G. Nelson, U. Weierstall, J. Spence, P. Schwander, L. Pollack, P. Fromme, A. Ourmazd, G. N. Phillips, Jr., M. Schmidt, *Struct. Dyn.* **2016**, 4, 044003; b) M. A. Wilson, *Annu. Rev. Biophys.* **2022**, 51, 79–98; c) M. Suga, A. Shimada, F. Akita, J.-R. Shen, T. Tosha, H. Sugimoto, *Biochim. Biophys. Acta Gen. Subj.* **2020**, 1864,



- 129466; d) M. A. Hough, R. L. Owen, *Curr. Opin. Struct. Biol.* **2021**, *71*, 232–238.
- [13] R. C. Nguyen, Y. Yang, Y. Wang, I. Davis, A. Liu, *ACS Catal.* **2019**, *10*, 1628–1639.
- [14] A. Perkins, D. Parsonage, K. J. Nelson, O. M. Ogbay, P. H.-Y. Cheong, L. B. Poole, P. A. Karplus, *Structure* **2016**, *24*, 1668–1678.
- [15] a) K. Kühnel, E. Derat, J. Terner, S. Shaik, I. Schlichting, *Proc. Natl. Acad. Sci. USA* **2007**, *104*, 99–104; b) P. K. Singh, P. Sharma, A. Bhushan, P. Kaur, S. Sharma, T. P. Singh, *J. Inorg. Biochem.* **2021**, *220*, 111461; c) J. Marangon, H. D. Correia, C. D. Brondino, J. J. G. Moura, M. J. Romão, P. J. González, T. Santos-Silva, *PLoS One* **2014**, *8*, e83234; d) J. Porta, A. Vahedi-Faridi, G. E. O. Borgstahl, *J. Mol. Biol.* **2010**, *399*, 377–384; e) H. P. Hersleth, B. Dalhus, C. Görbitz, K. Andersson, *J. Biol. Inorg. Chem.* **2002**, *7*, 299–304; f) W. Melik-Adamyan, J. Bravo, X. Carpena, J. Switala, M. J. Maté, I. Fita, P. C. Loewen, *Proteins* **2001**, *44*, 270–281; g) Y. Wang, I. Davis, I. Shin, H. Xu, A. Liu, *J. Am. Chem. Soc.* **2021**, *143*, 4680–4693.
- [16] a) S. G. Bell, W. Yang, A. B. H. Tan, R. Zhou, E. O. D. Johnson, A. Zhang, W. Zhou, Z. Rao, L.-L. Wong, *Dalton Trans.* **2012**, *41*, 8703–8714; b) S. G. Bell, R. Zhou, W. Yang, A. B. H. Tan, A. S. Gentleman, L.-L. Wong, W. Zhou, *Chem. Eur. J.* **2012**, *18*, 16677–16688; c) T. Coleman, R. R. Chao, J. B. Bruning, J. J. De Voss, S. G. Bell, *RSC Adv.* **2015**, *5*, 52007–52018; d) T. Coleman, S. H. Wong, M. N. Podgorski, J. B. Bruning, J. J. De Voss, S. G. Bell, *ACS Catal.* **2018**, *8*, 5915–5927.
- [17] a) T. Coleman, A. M. Kirk, J. H. Z. Lee, D. Z. Doherty, J. B. Bruning, E. H. Krenske, J. J. D. Voss, S. G. Bell, *ACS Catal.* **2022**, *12*, 1258–1267; b) T. Coleman, J. Z. H. Lee, A. M. Kirk, D. Z. Doherty, M. N. Podgorski, D. K. Pinidiya, J. B. Bruning, J. J. De Voss, E. H. Krenske, S. G. Bell, *Chem. Eur. J.* **2022**, *28*, e202201895; c) T. Coleman, D. Z. Doherty, T. Zhang, M. N. Podgorski, R. Qiao, J. H. Z. Lee, J. B. Bruning, J. J. De Voss, W. Zhou, S. G. Bell, *Chem. Asian J.* **2022**, *17*, e202200986; d) M. N. Podgorski, T. Coleman, L. R. Churchman, J. B. Bruning, J. J. De Voss, S. G. Bell, *Chem. Eur. J.* **2022**, *28*, e202202428.
- [18] a) M. N. Podgorski, J. S. Harbort, T. Coleman, J. E. Stok, J. A. Yorke, L.-L. Wong, J. B. Bruning, P. V. Bernhardt, J. J. D. Voss, J. R. Harmer, S. G. Bell, *Biochemistry* **2020**, *59*, 1038–1050; b) J. H. Z. Lee, M. N. Podgorski, M. Moir, A. R. Gee, S. G. Bell, *Chem. Eur. J.* **2022**, *28*; c) T. Coleman, A. M. Kirk, R. R. Chao, M. N. Podgorski, J. S. Harbort, L. R. Churchman, J. B. Bruning, P. V. Bernhardt, J. R. Harmer, E. H. Krenske, J. J. D. Voss, S. G. Bell, *ACS Catal.* **2021**, *11*, 1995–2010.
- [19] M. N. Podgorski, J. S. Harbort, J. H. Z. Lee, G. T. H. Nguyen, J. B. Bruning, W. A. Donald, P. V. Bernhardt, J. R. Harmer, S. G. Bell, *ACS Catal.* **2022**, *12*, 1614–1625.
- [20] a) J. Akter, T. P. Stockdale, S. A. Child, J. H. Z. Lee, J. J. De Voss, S. G. Bell, *J. Inorg. Biochem.* **2023**, *244*, 112209; b) J. Akter, E. F. Hayball, S. G. Bell, *Catal. Sci. Technol.* **2023**; c) A. R. Gee, I. S. J. Stone, T. P. Stockdale, T. L. Pukala, J. J. De Voss, S. G. Bell, *Chem. Commun.* **2023**, *59*, 13486–13489.
- [21] T. Coleman, R. R. Chao, J. J. D. Voss, S. G. Bell, *Biochim. Biophys. Acta Proteins Proteomics* **2016**, *1864*, 667–675.
- [22] K. Dornvil, I. Davis, A. J. Fielding, J. R. Terrell, L. Ma, A. Liu, *J. Biol. Chem.* **2017**, *292*, 13645–13657.
- [23] S. G. Bell, E. Orton, H. Boyd, J.-A. Stevenson, A. Riddle, S. Campbell, L.-L. Wong, *Dalton Trans.* **2003**, 2133–2133.
- [24] W. M. Atkins, S. G. Sligar, *J. Biol. Chem.* **1988**, *263*, 18842–18849.
- [25] M. Schmidt, *Crystals* **2020**, *10*, 116–116.
- [26] C. Stohrer, S. Horrell, S. Meier, M. Sans, D. von Stetten, M. Hough, A. Goldman, D. C. F. Monteiro, A. R. Pearson, *Acta Crystallogr. Sect. D* **2021**, *77*, 194–204.
- [27] E. Chovancova, A. Pavelka, P. Benes, O. Strnad, J. Brezovsky, B. Kozlikova, A. Gora, V. Sustr, M. Klvana, P. Medek, L. Biedermannova, J. Sochor, J. Damborsky, *PLoS Comput. Biol.* **2012**, *8*, e1002708–e1002708.
- [28] P. Zhao, F. Kong, Y. Jiang, X. Qin, X. Tian, Z. Cong, *J. Am. Chem. Soc.* **2023**, *145*, 5506–5511.
- [29] L. J. Bailey, B. G. Fox, *Biochemistry* **2009**, *48*, 8932–8939.
- [30] R. C. Nguyen, I. Davis, M. Dasgupta, Y. Wang, P. S. Simon, A. Butryn, H. Makita, I. Bogacz, K. Dornvil, P. Aller, A. Bhowmick, R. Chatterjee, I.-S. Kim, T. Zhou, D. Mendez, D. W. Paley, F. Fuller, R. Alonso Mori, A. Batyuk, N. K. Sauter, A. S. Brewster, A. M. Orville, V. K. Yachandra, J. Yano, J. F. Kern, A. Liu, *J. Am. Chem. Soc.* **2023**, *145*, 25120–25133.
- [31] N. P. Cowieson, D. Aragao, M. Clift, D. J. Ericsson, C. Gee, S. J. Harrop, N. Mudie, S. Panjikar, J. R. Price, A. Riboldi-Tunnicliffe, R. Williamson, T. Caradoc-Davies, *J. Synchrotron Radiat.* **2015**, *22*, 187–190.
- [32] T. G. G. Batty, L. Kontogiannis, O. Johnson, H. R. Powell, A. G. W. Leslie, *Acta Crystallogr. Sect. D* **2011**, *67*, 271–281.
- [33] P. R. Evans, G. N. Murshudov, *Acta Crystallogr. Sect. D* **2013**, *69*, 1204–1214.
- [34] M. D. Winn, C. C. Ballard, K. D. Cowtan, E. J. Dodson, P. Emsley, P. R. Evans, R. M. Keegan, E. B. Krissinel, A. G. W. Leslie, A. McCoy, S. J. McNicholas, G. N. Murshudov, N. S. Pannu, E. A. Potterton, H. R. Powell, R. J. Read, A. Vagin, K. S. Wilson, *Acta Crystallogr. Sect. D* **2011**, *67*, 235–242.
- [35] A. J. McCoy, R. W. Grosse-Kunstleve, P. D. Adams, M. D. Winn, L. C. Storoni, R. J. Read, *J. Appl. Crystallogr.* **2007**, *40*, 658–674.
- [36] P. Emsley, B. Lohkamp, W. G. Scott, K. Cowtan, *Acta Crystallogr. Sect. D* **2010**, *66*, 486–501.
- [37] P. D. Adams, P. V. Afonine, G. Bunkóczi, V. B. Chen, I. W. Davis, N. Echols, J. J. Headd, L.-W. Hung, G. J. Kapral, R. W. Grosse-Kunstleve, A. J. McCoy, N. W. Moriarty, R. Oeffner, R. J. Read, D. C. Richardson, J. S. Richardson, T. C. Terwilliger, P. H. Zwart, *Acta Crystallogr. Sect. D* **2010**, *66*, 213–221.
- [38] a) T. C. Terwilliger, R. W. Grosse-Kunstleve, P. V. Afonine, N. W. Moriarty, P. D. Adams, R. J. Read, P. H. Zwart, L.-W. Hung, *Acta Crystallogr. Sect. D* **2008**, *64*, 515–524; b) P. V. Afonine, N. W. Moriarty, M. Mustyakimov, O. V. Sobolev, T. C. Terwilliger, D. Turk, A. Urzhumtsev, P. D. Adams, *Acta Crystallogr. Sect. D* **2015**, *71*, 646–666.
- [39] R. Lonsdale, J. Oláh, A. J. Mulholland, J. N. Harvey, *J. Am. Chem. Soc.* **2011**, *133*, 15464–15474.

Manuscript received: October 10, 2023

Accepted manuscript online: November 16, 2023

Version of record online: December 15, 2023